

## MIT Open Access Articles

*Glycomics-based analysis of chicken red blood cells provides insight into the selectivity of the viral agglutination assay*

The MIT Faculty has made this article openly available. **Please share** how this access benefits you. Your story matters.

**Citation:** Aich, Udayanath, Nia Beckley, Zachary Shriver, Rahul Raman, Karthik Viswanathan, Sven Hobbie, and Ram Sasisekharan. "Glycomics-Based Analysis of Chicken Red Blood Cells Provides Insight into the Selectivity of the Viral Agglutination Assay." FEBS Journal 278, no. 10 (April 20, 2011): 1699–1712.

**As Published:** <http://dx.doi.org/10.1111/j.1742-4658.2011.08096.x>

**Publisher:** John Wiley & Sons, Inc

**Persistent URL:** <http://hdl.handle.net/1721.1/89155>

**Version:** Author's final manuscript: final author's manuscript post peer review, without publisher's formatting or copy editing

**Terms of use:** Creative Commons Attribution-Noncommercial-Share Alike





Published in final edited form as:

*FEBS J.* 2011 May ; 278(10): 1699–1712. doi:10.1111/j.1742-4658.2011.08096.x.

## GLYCOMICS-BASED ANALYSIS OF CHICKEN RED BLOOD CELLS PROVIDES INSIGHT INTO THE SELECTIVITY OF THE VIRAL AGGLUTINATION ASSAY

Udayanath Aich<sup>1</sup>, Nia Beckley<sup>1</sup>, Zachary Shriver<sup>1</sup>, Rahul Raman<sup>1</sup>, Karthik Viswanathan<sup>1</sup>, Sven Hobbie<sup>2</sup>, and Ram Sasisekharan<sup>1,2,\*</sup>

<sup>1</sup>Harvard-MIT Division of Health Sciences & Technology, the Koch Institute for Integrative, Cancer Research and the Department of Biological Engineering, Massachusetts Institute of Technology, Cambridge, MA 02139

<sup>2</sup>Singapore-MIT Alliance for Research and Technology, Centre for Life Sciences Singapore 117456

### SUMMARY

Agglutination of red blood cells, including chicken RBCs (cRBCs), have been used extensively to estimate viral titer, to screen glycan-receptor binding preference, and to assess the protective response of vaccines. While enjoying widespread use, it is known that some virus strains do not agglutinate RBCs. To address these underlying issues and increase the usefulness of cRBCs as tools to study viruses, such as influenza, we analyzed the cell surface N-glycans of cRBCs. Based on the results from complementary analytical strategies including mass spectroscopy, 1D and 2D-NMR spectroscopy, exoglycosidase digestions and HPLC profiling, we report here the major glycan structures present on cRBCs. By comparing the glycan structures of cRBCs to those of representative human upper respiratory cells, we offer a possible explanation for the fact that certain influenza strains do not agglutinate cRBCs, using specific human-adapted influenza hemagglutinins as examples. Finally, recent understanding of the role of various glycan structures in high affinity binding to influenza hemagglutinins provides context to our findings [1, 2]. These results illustrate that the field of glycomics can provide important information with regards to experimental systems used to characterize, detect, and study viruses.

### Keywords

Influenza; glycans; mass spectrometry; nuclear magnetic resonance

### INTRODUCTION

Existing assays used to quantify virus isolates and to assess the protective response of vaccines can be grouped into two categories; assays that “count” virus (or infectious) particles and assays which measure the binding of a virus particle to a cell, representative of the first step in the infection cycle. In the former category, assays include the assessment of plaques formed on a monolayer of mammalian cells, typically MDCK cells, as well as direct characterization or quantification of viral genome copies through PCR [3–5]. In the latter category, the most routinely used assay is the hemagglutination assay [6] where the ability of a given virus to bind to and agglutinate red blood cells (RBCs) is measured.

\*Address correspondence to: Ram Sasisekharan, Ph.D., 77 Massachusetts Avenue E25-519, Cambridge, MA 02139. Fax: 617-258-9409; rams@mit.edu.

In the case of influenza, for example, the hemagglutination assay takes advantage of the fact that hemagglutinin (HA) on the surface of human-adapted viruses typically binds to specific sialylated glycans on the surface of epithelial cells of the human upper respiratory tract, the key first step in the infection cycle [7]. RBCs, also possessing cell surface, sialylated glycans, act as a surrogate for this binding event. Agglutination of RBCs occurs when addition of a limiting amount of virus results in “crosslinking” of RBCs through binding of multiple RBCs to HAs present on a single virus; measurement of various concentrations of solutions can then be used to quantify viral titer. Additionally, introduction of antisera capable of neutralizing a viral strain reduces the ability of virus to agglutinate RBCs. In this manner, the protective effect of vaccines can be assessed. The agglutination assay has a number of advantages, including rapid turnaround time, easy readout, and benchmarked results with well-characterized virus strains. These considerable advantages have resulted in widespread adoption of this assay format.

Given the widespread use of RBCs, specifically those from chicken (cRBCs) as a tool, it is essential to understand to what extent its glycan repertoire recapitulates the receptors for human-adapted influenza strains (*i.e.* glycans of the human upper respiratory tract). This question becomes especially important in that previous studies have shown that various human-adapted virus strains and their mutants fail to agglutinate cRBCs. In one study, it was found that the A/Fujian/411/02 H3N2 virus, responsible for the unusually severe flu season of 2003–2004, did not efficiently agglutinate cRBCs [8]. This same lack of binding has been shown for other strains as well [9, 10].

Therefore, through a combination of analytical techniques including MALDI-MS, HPLC, exoglycosidase treatment, MS/MS and 1D and 2D-HSQC NMR, we report here a detailed characterization of the *N*-linked glycans present on the surface of cRBCs. We chose to look specifically at the *N*-glycan repertoire due to the fact that we have previously provided detailed characterization of the *N*-linked sialylated glycan receptors expressed on the cell surface of human bronchial epithelial cells (HBE), a natural target for infection by human-adapted influenza A viruses [11, 12]. By comparing the fine structure attributes such as degree and extent of branching and relative abundance of  $\alpha 2 \rightarrow 3$  and  $\alpha 2 \rightarrow 6$  terminal sialic acids between cRBCs and HBEs, our study provides insights into the inability of some human-adapted influenza viruses to agglutinate cRBCs. Defining the glycans present on the surface of cRBCs will allow for the design of strategies to either optimize the agglutination assay or design alternative strategies for the detection and quantification of virus strains. Additionally, we anticipate our strategy to integrate multiple analytical methods can be used to discern the structure of *N*-linked glycans obtained from other cell types and thus will prove useful to interrogate the role of glycans in a variety of disease processes.

## RESULTS

To provide a context to our studies, we examined the ability of two well-characterized HAs from prototypic, pandemic influenza strains, A/South Carolina/1/1918 H1N1 (SC18, 1918 pandemic) and A/Albany/6/1958 H2N1 (Alb58, 1957 pandemic), to agglutinate cRBCs. These HAs, both from human-adapted, pandemic viruses, have distinct glycan binding characteristics (Supplemental Fig. S1). While both strains bind with high affinity to a subset of  $\alpha 2 \rightarrow 6$  sialylated glycans able to adopt an *umbrella* topology, associated with human-adaptation [11, 12], SC18 binding is restricted to only glycans of this type, whereas Alb58 also binds other  $\alpha 2 \rightarrow 6$  and  $\alpha 2 \rightarrow 3$  sialylated glycans [13]. In the context of the agglutination assay, Alb58 HA agglutinated cRBCs at concentrations as low as 6.25  $\mu\text{g}/\text{mL}$  (Supplemental Fig. S2A). Conversely, SC18 HA does not agglutinate cRBCs in the concentration range tested (up to 400  $\mu\text{g}/\text{mL}$ ) (Supplemental Fig. S2B). Taken together with previous reports [8–10], this data indicates that the glycans of cRBCs may not be

representative of the physiological receptors for human-adapted influenza strains. Therefore, structural analysis of the cell surface glycans and comparison of these structures to those present on human upper respiratory epithelium is critical to understand the output of the agglutination assay, as well as to provide information on its strengths and limitations.

### Release and MALDI-MS Analysis of N-Glycans from Chicken Red Blood Cells

N-glycans were isolated from both bovine fetuin, used as a control protein, and from the surface of chicken red blood cells (cRBCs). PNGase F was used for enzymatic cleavage of N-glycans as it releases most protein-bound N-linked carbohydrates from animal-derived cells [14]. Post-purification, but prior to labeling, N-glycans were characterized by orthogonal analytical techniques including MALDI-MS and NMR.

To obtain preliminary information about the glycan pattern in terms of sugar composition and possible branching patterns of cRBC glycans, MS profiling was performed. MS-based strategies offer a sensitive tool to determine glycan composition [15], and the resulting glycan map provides an overall structural fingerprint of the sample. MALDI-MS analysis of released N-glycans from cRBCs indicates the presence of a wide range of structures; tentative assignments of molecular ions are reported in Fig. 1. Additionally, with appropriate sample work-up and analysis, semi-quantitative information can also be obtained from this analysis through the use of soft ionization conditions [16], which have been optimized for the detection of acidic, sialylated structures. To validate the accuracy of the method, analysis of fetuin N-glycans under identical experimental conditions was performed and compared with previously reported structures [17] and indicated good agreement, both qualitatively and quantitatively. This analysis provided us with an overall set of glycan compositions; additional analyses were performed to extend initial results and provide more detailed information on the glycan sequence, including linkages and branching patterns.

### Analysis of cRBC glycans by $^1\text{H}$ NMR

To determine the most relevant glycan sequences for each composition, we completed additional MS and NMR-based analysis of the cRBC glycan pool. In addition to identification and quantification of other monosaccharides, we sought to characterize the overall sialic acid content, to benchmark our analysis to existing studies using lectin staining [10, 18]. Additionally such an analysis is particularly important with reference to the cRBC/influenza system, since it is known that human-adapted HAs bind to  $\alpha 2 \rightarrow 6$  linked sialic acids, while avian-adapted subtypes bind  $\alpha 2 \rightarrow 3$ -linked sialic acids [19–21].

To obtain quantitative information regarding the sialic acid linkages in cRBCs, we used separate strategies which together provide overlapping information. First, two different glycosidases were used to digest glycans – Sialidase S, which cleaves  $\alpha 2 \rightarrow 3$  and  $\alpha 2 \rightarrow 8$  linked terminal sialic acid moieties, leaving intact  $\alpha 2 \rightarrow 6$  linked sialic acid – and Sialidase A [22], which cleaves  $\alpha 2 \rightarrow 3$ ,  $\alpha 2 \rightarrow 6$ , and  $\alpha 2 \rightarrow 8$  linked sialic acids. In combination with MALDI MS analysis, enzymatic treatment was used to obtain qualitative information about the overall distribution of sialic acid linkages among the compositions observed. Secondly, to obtain quantitative information, NMR spectroscopy was carried out. As above, N-linked glycans from fetuin were used as a standard sample to assess method accuracy. With fetuin N-linked glycans, treatment with Sialidase A and Sialidase S and subsequent assessment by MALDI-MS indicates the presence of a mixture of  $\alpha 2 \rightarrow 3$  and  $\alpha 2 \rightarrow 6$  linked sialic acids (Supplemental Fig. S3), which are evenly distributed across the glycan species.  $^1\text{H}$ -NMR spectra of this N-glycan pool indicates the presence of peaks at 1.80 and 1.72 ppm due to the H3 (axial) proton of  $\alpha 2 \rightarrow 3$  and  $\alpha 2 \rightarrow 6$  linked sialic acid, respectively. Integration of these clearly resolved signals indicates that the amount of  $\alpha 2 \rightarrow 3$  and  $\alpha 2 \rightarrow 6$  linked glycans is approximately 56% and 44%, respectively (Supplemental Fig. S4).

Fig. 2A shows the MALDI-TOF MS data of Sialidase S-treated cRBC samples. Overall, these results demonstrate that cRBCs also contain a mixture of  $\alpha 2 \rightarrow 3$  and  $\alpha 2 \rightarrow 6$  linked sialic acids. Three major peaks appeared at 2134.7, 2296.9 and 2499.8 after treatment of the cRBC N-glycan pool with Sialidase S. The  $m/z$  value of 2134.76, a biantennary glycan with one sialic acid and one bisecting GlcNAc, is likely derived from the parental species at 2426.6 upon release of one sialic acid, suggesting both  $\alpha 2 \rightarrow 3$  and  $\alpha 2 \rightarrow 6$  linked sialic acids are present on the glycan. The  $m/z$  value at 2296.9 is representative of a triantennary glycan with one sialic acid and is likely derived from a parental species with an  $m/z$  value of 2880.5 through release of two sialic acid monosaccharides. Alternatively, the same species could be obtained from  $m/z$  of 2589.1 upon release of one sialic acid. In either case partial release of sialic acid suggests the presence of both  $\alpha 2 \rightarrow 3$  and  $\alpha 2 \rightarrow 6$  linked sialic acids on glycan species within the cRBC pool. Finally, the species at  $m/z$  2499.9, a triantennary glycan with one sialic acid and with one bisecting GlcNAc, is likely obtained from species at  $m/z$  of 2792.2 and 3083.8 by the release of one and two sialic acids, respectively. Quantitative  $^1\text{H-NMR}$  analysis of this sample also indicates the presence of a mixture of both  $\alpha 2 \rightarrow 3$  and  $\alpha 2 \rightarrow 6$  linkages, with the peaks at 1.80 and 1.76 ppm due to the H3 (axial) protons and peaks at 2.69 and 2.64 ppm due to H3 (equatorial) protons with measured integral ratio of 54: 46 (Fig. 2B).

### Additional $^1\text{H-NMR}$ and $^1\text{H-}^{13}\text{C}$ HSQC spectroscopic characterization of cRBCs

We also extended our NMR analysis to examine a number of other features within the cRBC glycan pool which are clearly resolved and can be used to assess overall structure, including identifying and quantifying the anomeric protons, the H-2 protons of mannose residues, the H-5 and H-6 protons of fucose residues, the N-acetyl protons of N-acetylglucosamine (GlcNAc), and the H3-equatorial and H3-axial protons of N-glycolylneuraminic acid (NeuGc) [23–26]. The  $^1\text{H-NMR}$  spectrum of cRBCs within the region of interest is shown in Fig. 3 and the list of important chemical shifts, along with a schematic of protons and probable assignments is shown in Supplemental Table S1. Within the cRBC N-glycan pool, we detect the presence of several important signatures, including the H-1 anomeric protons, the H-2 protons of Man ( $\delta$  4.05 to 4.25 ppm), and the methyl protons of the N-acetyl groups. In the spectrum, the presence of sialic acid is confirmed by the detection of a  $-\text{CH}_3$  signal around 2.07, proximate to the  $-\text{CH}_3$  signals for GlcNAc-2 and GlcNAc-7 (Table S1) [27]. Within this same region, the presence of two additional species at 2.03–2.06 ppm are likely due to  $-\text{CH}_3$  signals of GlcNAc-5 and GlcNAc-5' and point to the presence of both bi- and triantennary glycan structures within the cRBC pool. This interpretation was confirmed by identifying the H-1 and H-2 chemical shifts of mannose monosaccharides within the spectrum. In this case, the fingerprint chemical shift of the H-2 proton of Man $\alpha 1 \rightarrow 6$  at 4.13 arises from mannose in biantennary structures, whereas, the peaks at 4.07 ppm indicate the presence of H-2 protons of Man $\alpha 1 \rightarrow 6$  within tri-antennary structures.

The chemical shifts of the anomeric protons of GlcNAc-2, GlcNAc-5, GlcNAc-5', galactose (Gal)-6, Gal-6' and Gal-8 appear in the region of 4.40 to 4.75 ppm (see Table S1 for naming). Specifically, the anomeric proton of GlcNAc-2 appears at 4.62 ppm; the GlcNAc-5 and GlcNAc-5' anomeric protons appear at 4.56–4.59. The signal at 4.54 ppm can be attributed to the anomeric proton of GlcNAc-7; however, the absence of a signal at 5.56 ppm (which would be assigned to GlcNAc-7', if present) indicates the relative absence of tetraantennary structures. According to previous studies[27], the presence of an extended lactosamine repeat is characterized by signals for the anomeric protons of the two monosaccharide units - GlcNAc- $\beta$  and Gal $\beta$  - at 4.70 and 4.56 ppm, respectively. While likely absent from the proton spectrum of cRBC glycans, the presence of a prevalent proton signal from the anomeric position of Man  $\beta 1 \rightarrow 4$  necessitated running an HSQC experiment to resolve this region of the spectrum to determine the presence or absence of signals (see

below). Taken together, the results from NMR indicate there are likely both bi-, and triantennary structures within the cRBC N-glycan pool with a mixture of  $\alpha 2 \rightarrow 3$  and  $\alpha 2 \rightarrow 6$  linked sialic acids as well as structures containing bisecting GlcNAc.

First, to resolve all signals and ensure accurate quantification of the relative mole% of different monosaccharides, two-dimensional (2D)  $^1\text{H}$ - $^{13}\text{C}$  HSQC was carried out. As above, analysis was completed first on the N-glycan pool from bovine fetuin to ensure accuracy of analysis. The HSQC spectra with volume integration of the anomeric region is shown in Supplemental Fig. S5. The chemical shift of H-1 of GlcNAc-1 at 5.18 ppm showed a cross peak with C-1 carbon at  $\sim 90$  ppm, two dimensional volume integration of this signal was set to 1.00 as this signal, within the chitobiose core that is common to all *N*-linked glycans. A cross peak at 4.62 and 94 ppm is assigned to the GlcNAc-2. Man  $\alpha 1 \rightarrow 3$  showed a cross peaks at 5.11 and 99 ppm, whereas Man  $\alpha 1 \rightarrow 6$  showed a cross peaks at 4.8–4.9 and 97 ppm for H1/C1. Conversely, Man  $\beta 1 \rightarrow 4$  showed a cross peak at 4.73–4.77 and  $\sim 100$  ppm with a similar integration value. GlcNAc-5 and GlcNAc-5' had cross peaks at 4.57 and 99.2 ppm, with an integration value of  $\sim 2.00$ , confirm the presence of two protons. Notably, there is no indication of presence of extra cross peaks at 4.70 which would represent the GlcNAc portion of a lactosamine repeat.

Next, to obtain detailed structural information of N-glycans from cRBCs, we performed HSQC analysis of these N-glycans. Because the HSQC spectra of cRBCs displayed similar cross peak as discussed above for bovine fetuin, analysis was effectively benchmarked and simplified. In the case of the cRBC glycan pool, cross peaks due to GlcNAc-1, GlcNAc-2, GlcNAc-5, GlcNAc-5', Man  $\alpha 1 \rightarrow 3$  and Man  $\alpha 1 \rightarrow 6$  (Fig. 4) appeared in a similar position with equal integration. The presence of bi-antennary and tri-antennary was also confirmed by the detection of two different cross peaks at 4.58 and 4.54 ppm and  $\sim 99$  ppm, due to the presence of GlcNAc-5&5' and GlcNAc-7 respectively. The cross peak at 4.68 and 99 ppm is assigned to Man  $\beta 1 \rightarrow 4$ . Within the cRBC glycan pool there are no detectable cross peaks of either GlcNAc $\beta$  or Gal $\beta$ , indicating the absence of repeating lactosamine units.

### HPLC profiling of 2-aminobenzamide linked N-glycans mixture from cRBCs

To supplement the structural data obtained on the entire *N*-glycan pool, we labeled cRBC glycans with 2-aminobenzamide (2AB), separated them into oligosaccharide pools and quantified these pools using HPLC. N-glycans from fetuin were labeled and used as a standard to ensure a standardized analysis. Additionally, to ensure that the labeling reaction did not result in introduction of sample bias, both labeled and unlabeled cRBC glycans were profiled on HPLC by pulsed amperometric detection. Comparison of the profiles indicated no change in the number of peaks nor their relative area (data not shown). Finally, to calibrate the column with the solvent gradient system (Supplemental Table S2), a glucose homopolymer ladder is used for calibration. Each detected peak within the ladder is labeled with a glucose unit (gu) value as shown in Fig. 5A, similar to reported methods [28]. Subsequently, a mixture of three 2AB-labeled *N*-glycan standards (containing one, two, or three sialic acids) were used to benchmark the retention times of acidic N-glycans from cRBCs in our system. Peaks corresponding to these standards appeared between the retention times of 120–200 min (Fig. 5B). The area under curve for all three peaks are equivalent to the amount of each glycan injected, consistent with the fact that detection was largely determined by the label and independent of the attributes of the glycan to which it is attached. Given this, we sought to determine the amount of individual cRBC glycans by HPLC through use of a standard curve created by injecting amounts of the three standards that encompass the ranges of glycans present in the cRBC glycan pool (Supplemental Fig. S6).

2AB-labeled *N*-glycans were qualitatively and quantitatively assessed using this normal phase HPLC system. The 2AB-labeled glycans from fetuin appear at retention times between 120 to 200 min and displayed 10 major peaks, which matched the 10 major species observed through the MALDI-MS profile. Profiling of the cRBC *N*-glycans showed 12 major peaks in the retention time range of 120–200 min (Fig. 5C). The detailed peak retention time of each peak including annotation are shown in supplemental Table S3. Based on the standard curve as shown in Supplemental Fig. S6, the amount of glycan in each peak was calculated to estimate a percent recovery. The total glycan isolated by HPLC was calculated to be 91 picomoles (Table S3, ~ 90 % of the injected glycan of 102 picomole). Taken together with the control experiments outlined above, these results indicate that our quantitative measurements here can reasonably be correlated with quantitative measurements on the glycan pool, *i.e.* NMR and MALDI analysis. To complete the analysis of *N*-glycans, three separate, but complementary, approaches were taken. First, pools were automatically collected and subjected to MS analysis by MALDI TOF. Additionally, we completed sialidase treatment of the collected pools, to determine the distribution of sialic acid. Next, we completed on-line MS/MS analysis of the major species; some of these species were further analyzed by TOF/TOF to ensure accurate structural elucidation.

First, after HPLC profiling, several fractions were collected based on the retention time of individual peaks and glycans under the peaks and analyzed using MALDI-MS. The various 2AB linked glycans in each peak are shown in Supplemental Table S3. To examine sialic acid content, sialidase treatment of the 2-AB linked *N*-glycan pool from cRBCs was performed (Supplemental Fig. S7). HPLC analysis of the sample after enzymatic treatment with sialidase S showed that the retention time of some of the peaks remained the same, indicating no sialic acid cleavage, whereas there was the appearance of new peaks in retention time window of 5–55 mins (indicating sialic acid cleavage). Integration of the AUCs for each window confirms the presence of a mixture of  $\alpha 2 \rightarrow 3$  and  $\alpha 2 \rightarrow 6$  linked sialic acids, in a mixture of roughly 50/50, within the cRBC glycan pool.

There are eleven major *N*-glycan species that are observed in the cRBC pool. Based on their mass signature, NMR analysis, and enzymatic treatment, the most likely structure for two of these species, *viz.*, 2135.3 and 2426.6, can be assigned (Table 1). For the rest of the major species, LC-MS/MS was completed to assign structure. LC-MS/MS of the species with observed molecular masses of 2500.1, 2792.2, 2880.5, and 3083.8, in combination with the constraints obtained from the analysis of the *N*-glycan pool, enabled definitive assignment (Fig. 6A–D, Table 1). For two of the species, *viz.*, with observed masses of 2297.6 and 2589.1, the fragmentation patterns are consistent with two species, one with a lactosamine extension and one without (Supplemental Fig. S8). Based on the fact that the NMR analysis, both mono- and bidimensional, indicated the absence of lactosamine repeats, the most likely structure for both is the first indicated. To confirm this, TOF/TOF analysis of 2297.6 yielded a fragmentation pattern consistent with this proposed structure. Taken together, the data thus strongly supports the structural assignment presented in Table 1.

Comparison of the glycans observed for human bronchial epithelial (HBE) cells with those present on cRBCs (Table 1) indicates some similarities; for example, both *N*-glycan pools have species with *m/z* signals at ~ 2224.0, 2297.6, 2589.1 and 2880.5. In contrast, many of the species observed for HBE's (*m/z* = ~2078.0, 2408.2, 2443.0, 2611.0, 2661.5, 2733.1, 2773.0, 2808.3, 2894.9, 2954.6, 3057.0, and 3097.0)[11] are either completely absent or are less prominent in cRBCs. Specifically the species with *m/z* signals at 2808.3, 3057.0 and 3097.0 were previously shown in HBEs to correspond to structures with lactosamine repeats terminated by sialic acid. Notably, such glycan motifs, polylactosamine extensions terminated by  $\alpha 2 \rightarrow 6$  sialic acid, can adopt a distinct *umbrella-like* topology that governs high-affinity binding to HA from human-adapted influenza viruses [11]. The most intense

peak in the analysis of cRBCs, at 2880.9, is present in HBEs as a minor component, and likely does not represent a structure containing a lactosamine repeat unit. Finally, inspection of Table 1 indicates that several prominent mass peaks present in cRBCs are absent or less abundant for HBEs. For example, the peak at  $m/z$  2135.3, represents a biantennary structure with a bisecting GlcNAc and lack of lactosamine repeats. Thus, beyond the presence of both  $\alpha 2 \rightarrow 3$  and  $\alpha 2 \rightarrow 6$  sialylation, the N-glycans of cRBCs do not recapitulate key properties of the physiological glycan species encountered by viruses, such as influenza.

## DISCUSSION

The widespread use of cRBC agglutination in influenza surveillance and research necessitates a complete understanding of the structures of the glycan receptors present on the surface of cRBCs. This is important both for understanding the limitations of the assay and for better interpretation of the hemagglutination assay results. In this study, distinct analytical approaches including combining 2D-NMR, HPLC profiling, and MS/MS analysis were employed to provide detailed structural information on cRBC glycans. Notably, while we often employed fetuin as a control, the quantitative analysis provided here goes beyond the several reports of glycans moieties in bovine fetuin [17, 29].

A combination of these analytical techniques showed that the glycan structures on cRBCs were found to possess both  $\alpha 2 \rightarrow 3$  and  $\alpha 2 \rightarrow 6$  linked sialic acid. Significantly, the analysis revealed an absence of lactosamine repeats, and the presence of bi- and triantennary structures. This is in contrast to the predominance of  $\alpha 2 \rightarrow 6$  sialylated glycans with lactosamine repeats on HBEs, including tetraantennary structures (Table 1). Taken together, these results indicate that the glycan repertoire of cRBCs is distinct from that of human upper respiratory cells which are the targets for infection by human adapted influenza A viruses. These results provide a context to possibly explain why certain human-adapted influenza strains do not agglutinate RBCs. We note that our analyses here focus on characterizing the N-linked glycans extracted from cRBCs. In addition to the fact that previous analysis of HBEs focused on the N-glycan pool, we find that sialylated N-glycans represent a substantial percentage of total sialylated glycans present on cRBCs. Apart from the predominantly non-sialylated O-glycans that are a part of ABH blood group antigens, cRBCs are known to have sialylated O-glycans attached to glycoproteins such as glycophorins [30]. Most of these sialylated O-linked glycans are terminated by  $\alpha 2 \rightarrow 3$ -linked sialic acid (typically terminating Core 1-type structure) and hence are likely not receptors for human-adapted influenza A viruses, which require the presence of  $\alpha 2 \rightarrow 6$  sialylation.

The difference in the N-linked glycan repertoire of cRBC and human epithelial cells limits the ability of agglutination assay to assess virus-host binding as highlighted by the results presented in Supplemental Fig. S1A. In previous studies, SC18 HA has demonstrated specific high-affinity binding only to 6'SLN-LN, an  $\alpha 2 \rightarrow 6$  motif with a polylactosamine repeat that is able to adopt an *umbrella* topology. On the other hand, while Alb58 also showed demonstrated high binding affinity to 6'SLN-LN (comparable to SC18 HA), it also bound to 6'SLN and other  $\alpha 2 \rightarrow 3$  sialylated glycans (Supplemental Fig. S1B). The observed difference in the ability of SC18 and Alb58 HA to agglutinate cRBC is explained by minimal presence of sialylated glycans with poly-lactosamine repeats in the cRBCs. Alb58 on the other hand binds to sialylated glycans with single lactosamines on the cRBCs and hence shows agglutination.

In summary, our studies have important implications in improving the use of RBC agglutination assays given that this assay still offers an easy readout for rapid screening. Using the combination of analytical techniques outlined here, it is possible to obtain fine



structural characterization of sialylated glycans expressed in RBCs from different sources. Such a detailed characterization of glycans from different RBCs would permit selection of the appropriate RBCs to screen avian-adapted and human-adapted viruses. Additionally, it would also allow for rational engineering of glycan structures on the RBC surface such as introducing additional enzymes that can generate lactosamine repeats prior to the terminal sialylation step instead of simply desialylating and resialylated cRBCs.

In addition to improving the use and interpretation of RBC agglutination assay our study also offers new possibilities for developing focused platforms to determine relative  $\alpha 2 \rightarrow 3$  and  $\alpha 2 \rightarrow 6$  sialylated glycan receptor-binding specificity and affinity which has been shown to be associated with the human adaptation of the influenza virus [11, 12]. Specifically, knowledge of the fine structure of the sialylated glycans from different cell types would permit generation of different glycan fractions from these cell types where each fraction would be characterized in terms of the predominance of a specific terminal sialic acid linkage and other features such as branch length and extent of branching. These defined glycan fractions can then be used for developing “natural” glycan array platforms [31] that can then be used to probe and quantify the binding specificities of HA from avian- and human-adapted viruses.

## MATERIALS AND METHODS

PNGase F (Glycerol Free) was obtained from NE BioLabs. Signal 2-AB Labeling Kit, Sialidase-A and sialidase-S were obtained from Prozyme. Bovine fetuin, SDS, 2-mercapto ethanol, acetonitrile, trifluoro acetic acid, ATT matrix, Nafion, SP20SS beads and H<sup>+</sup> dowex cation exchanger beads were obtained from Sigma-Aldrich. Calbiosorb beads (Cat. No. 206550) and protease inhibitor cocktail (Cat. No. 53914) were obtained from Calbiochem. Sep-pak @ C18 columns were obtained from Waters and ENV<sup>TM</sup>-Carb SPE tubes were from Supelco. C-RBC's were obtained from Rockland Chemicals, and D<sub>2</sub>O was obtained from Cambridge Isotope. All commercial reagents were used without further purification.

### N-Glycan release by PNGase F from Bovine Fetuin

For many of the assays presented here, bovine fetuin was used as a control, given that its glycan repertoire is well-characterized [17, 30]. About 1 mg of intact glycoprotein was dried by lyophilization. To this, 300  $\mu$ L of purified water was added to make a protein solution of  $\sim 3.3$  mg/mL. 50  $\mu$ l of 10X denaturing buffer was added to the vial and incubated in heat block at 100°C for  $\sim 10$  minutes. After cooling, 50  $\mu$ L of both 10X G7 reaction buffer and 10% NP-40 were added to the denatured protein and mixed well. Then 50  $\mu$ L PNGase F was added, after which, incubation at 37°C was carried out for about 24 hours. After deglycosylation, initial clean-up of the released glycans from the protein was completed by adding 500  $\mu$ l of Calbiosorb beads to remove SDS. At this point, the sample was further purified as described below.

### Red Blood Cell Surface Glycan Extraction

Glycans were extracted from the surface of cRBCs according to a modified version of a previously published protocol [11]. cRBCs preparations were diluted in PBS to obtain a concentration of approximately 400 million cells per mL. The following steps were then repeated twice; cells were spun down at 2,000g for 10 minutes at 4°C, the supernatant was aspirated, and the pellet was resuspended in 0.5mL of PBS + 1% protease inhibitor. Cells were then lysed for 15 minutes under gentle agitation at room temperature in 500  $\mu$ L of deionized water containing 1% protease inhibitor. The suspension was then spun down at 2000g for 10 minutes at 4°C and resuspended in 500  $\mu$ L of PBS + 1% protease inhibitor. An additional spin down cycle was performed using the same buffer volume at 4,000g for 10

minutes at 4°C. The supernatant was removed, and the pellet was resuspended in 20 µl of deionized water and 230 µl of an aqueous solution of 1% SDS + 20 mM 2-mercaptoethanol. The suspended pellets were boiled in a hot water bath for 10 minutes, after which 40 µl of 10% NP40 (PNGase F Kit), 40 µl of G7 Buffer (PNGase F Kit), and 10 µl of PNGase F were added to the mixture. The pellets were incubated for 24 hours at 37°C under gentle agitation. After incubation, 100 µl of Calbiosorb beads were added to the mixture to remove SDS, and this mixture was incubated for 15 minutes under gentle agitation at room temperature. At this point, the sample was further purified as described below.

### Purification of glycans

After digestion with PNGase F, samples were treated with prewashed calbiosorb beads, centrifuged, and the supernatant was added to an equilibrated Sep-Pak C18 column, according to the manufacturer's instructions. Then, 6 mL of 5% acetonitrile, 0.05% TFA was used to elute the sample. After lyophilization and drying, the sample was resuspended in 1 mL of water and added to a pre-equilibrated ENV™-Carb SPE tube. After washing with 0.05% TFA in water, and 5% acetonitrile, 0.05 % TFA in water, N-glycans were eluted in 50% acetonitrile/ water with 0.1% TFA. The purified glycan prep was lyophilized and reconstituted in 40 µL of water.

### 2-Amino benzamide (2AB) labeling of N-glycans

Selected N-glycan reactions were fluorescently tagged using the Signal™ 2-AB labeling kit. Briefly, the reaction was carried out according to the manufacturers' instructions at 65°C for 3 hours. After completion, the samples were purified by using a pre-equilibrated GlykoClean G Cartridge. The labeling reaction was added to the column and washed with 96% acetonitrile/mili-Q water. Labeled glycans were eluted with mili-Q water (6 × 1mL).

### Glycan MS Analysis by MALDI-MS spectroscopy

All glycans were analyzed using the Voyager DE-STR MALDI-TOF. The sample and matrix were combined in a ratio of 1:9, respectively. Nafion (1 µl) was spotted on the plate and allowed to dry for ~5 minutes. The matrix-sample mixture was then placed on top of the Nafion spot and allowed to dry in a humidity-controlled chamber (humidity 23%). The following parameters were used for analysis: negative and linear Mode, 22,000V Accelerating Voltage, 93% Grid Voltage, 0.3% Guide Wire, 150 nsec Delay. Peaks were calibrated as non-sodiated species using external glycan standards. Proposed glycan compositions for each peak were determined by imputing the peak masses into the GlycoMod software (<http://ca.expasy.org/tools/glycomod/>), which calculates all mathematically possible glycan compositions for a given mass.

### HPLC analysis of 2AB linked N-glycans using Glyco Sep N column

Labeled glycans were separated and quantified using a GlycoSep™ N HPLC column and a two solvent, gradient system (Solvent A is 100 % acetonitrile; Solvent B is 50 mM ammonium formate pH 4.4) with UV and fluorescence detection. The gradient table for the elution of 2AB linked N-glycans from cRBCs including glucose homopolymer and N-glycan standards is shown in Supplemental Table S2. Prior to the HPLC profiling of N-glycans from cRBCs, the column and gradient system was verified using Glucose homopolymer. Furthermore, to obtain accurate retention times for the various N-glycan species, a standard mixture of known 2AB linked N-glycans (2AB-A1, 2AB-A2 and 2AB-A3) was injected to the HPLC. Standard N-glycans and those from cRBCs typically eluted in the 120 to 200 retention time window. The number of peaks and their area under curve was used for qualitative and quantitative estimation of N-linked structural pools present in cRBCs. Additionally, during HPLC profiling several fractions were collected. Subsequently,

solvents were removed by speed-vac and re-suspended with a minimum amount of water, followed by structural characterization of each individual peaks using MALDI-MS. The mass peaks obtain from each fraction were also analyzed based on the standard MALDI-MS GlycoMod software. The possible 2AB linked glycans in each fraction were assessed based on the N-glycan biosynthesis annotation.

### NMR study of N-glycans

The isolated and purified N-glycans were deuterium exchanged using 99 % D<sub>2</sub>O (three times) and dried by lyophilization. The dried substance were dissolved in 400 μL of Deuterium oxide (100 %) and transferred to a 5 mm NMR tube. <sup>1</sup>H NMR spectra were recorded in a Bruker 600 MHz NMR with a cryo-probe using the Topspins program. 2D-HSQC <sup>1</sup>H-<sup>13</sup>C-NMR spectra were recorded without spinning with the standardized water frequency O1, p1 (10<P1<16) and D1 (for N-glycans, D1 = 2) values.

### Assessment of Sialic Acid Linkages

To purified N-glycan samples, 10 μL of 5X reaction buffer and 7 μL of sialidase A from *Arthrobacter Ureafaciens* or Sialidase S from *Streptococcus Pneumoniae* (Prozyme) was added and incubated at 37°C for 18 h. The reaction mixture was then heated to 100°C on a heat block for 5 min to inactivate the enzyme. Subsequently, prior to analysis, the glycans were purified by micro columns using SP20SS and H+ Dowex Cation Exchanger beads. Additionally, sialic acid quantification was performed by conversion of the released sialic acid to pyruvic acid. The released hydrogen peroxide was quantified using standard UV/fluorescence detection methods. The assay was carried out using the protocol supplied with the kit. A standard curve obtained using a sialic acid standard was used to quantify detected sialic acid.

### LC-MS/MS Analysis

Unlabeled or 2-AB labeled glycans were subjected to LC-MS analysis. LC was carried out using an Ultimate 3000 LC system (Dionex) using a C-18 Reverse Phase column (1.8 μm; 2.1mm × 50mm). The mobile phases employed included water/0.1% acetic acid (Solvent A) and 5% acetonitrile in water with 0.1% acetic acid (Solvent B). A gradient of B over ~60 min was used for N-glycan analysis. The flow-rate used was 250μL/min from the LC system through a splitter adjusted to obtain a 12μL/min flow into the LTQ ion-trap mass spectrometer from Thermo Fisher-Scientific. The LTQ MS was operated in positive mode with ESI voltage of 3.9kV and capillary temperature of 200°C. Triple play data dependent scanning method was used where 1 MS scan (5 μscans averaged) was followed by a zoom scan and MS<sup>n</sup> on the top eight most intense ions. Ions from m/z 480–2000 were selected.

### MALDI TOF/TOF

In addition to LC-MS/MS analysis, we also completed TOF/TOF analysis of selected peaks to confirm structure using MDS Sciex 4800 MALDI TOF/TOF™ instrument and controlled by the 4000 series explorer™ software. TOF/TOF fragmentation spectra were recorded using negative-ion linear mode with standardized MS/MS acquisition and processing methods after tuning of the instrument. TOF/TOF spectra are obtained in 1kV operating mode with relative resolution of 50 FWHM and laser intensity of 5600 with 400 total shots.

### Supplementary Material

Refer to Web version on PubMed Central for supplementary material.

## Acknowledgments

This work was supported by Singapore-MIT Alliance for Research and Technology

## Abbreviations used

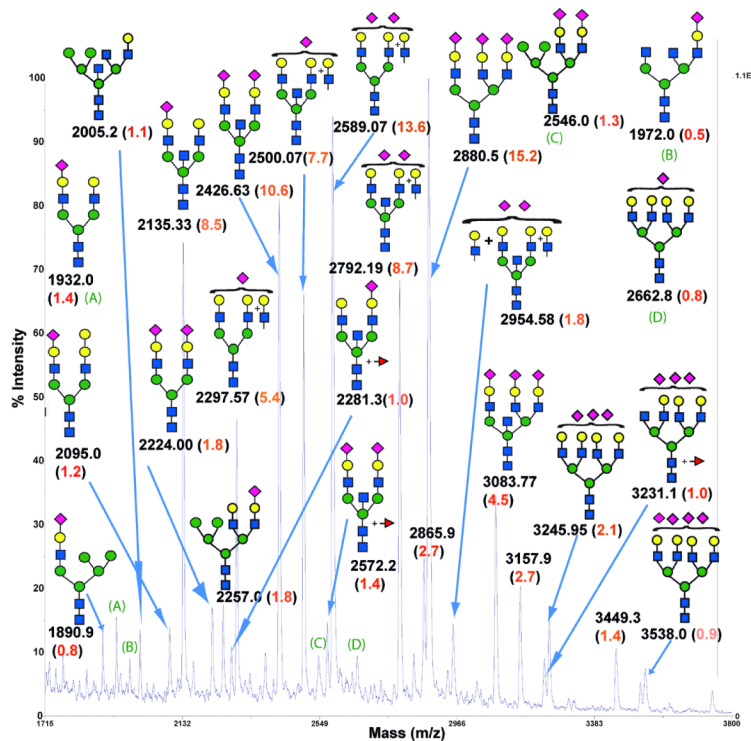
<b>cRBCs</b>	chicken red blood cells
<b>HAs</b>	hemagglutinin proteins
<b>MDCK</b>	madindarby canine kidney
<b>PCR</b>	polymerase chain reaction
<b>MALDI</b>	matrix-assisted laser desorption/ionization
<b>SDS</b>	sodium dodecyl sulfate
<b>D<sub>2</sub>O</b>	deuterium oxide
<b>TFA</b>	trifluoroacetic acid
<b>HSQC</b>	heteronuclear single quantum coherence
<b>ATT</b>	6-aza-2-thiothymine
<b>GlcNAc</b>	N-acetyl glucosamine
<b>Gal</b>	galactose
<b>Man</b>	mannose
<b>NeuAc</b>	N-acetyl Neuraminic acid
<b>Fuc</b>	fucose

## REFERENCES

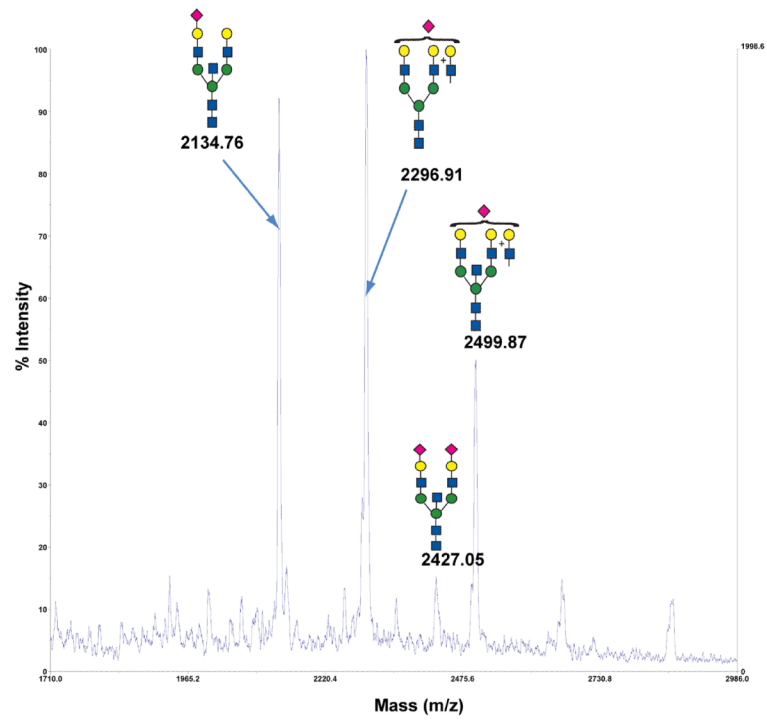
1. Hensley SE, Das SR, Bailey AL, Schmidt LM, Hickman HD, Jayaraman A, Viswanathan K, Raman R, Sasisekharan R, Bennink JR, Yewdell JW. Hemagglutinin receptor binding avidity drives influenza A virus antigenic drift. *Science*. 2009; 326:734–6. [PubMed: 19900932]
2. Maines TR, Jayaraman A, Belser JA, Wadford DA, Pappas C, Zeng H, Gustin KM, Pearce MB, Viswanathan K, Shriver ZH, Raman R, Cox NJ, Sasisekharan R, Katz JM, Tumpey TM. Transmission and pathogenesis of swine-origin 2009 A(H1N1) influenza viruses in ferrets and mice. *Science*. 2009; 325:484–7. [PubMed: 19574347]
3. Boon AC, French AM, Fleming DM, Zambon MC. Detection of influenza a subtypes in community-based surveillance. *J Med Virol*. 2001; 65:163–70. [PubMed: 11505459]
4. Amano Y, Cheng Q. Detection of influenza virus: traditional approaches and development of biosensors. *Anal Bioanal Chem*. 2005; 381:156–64. [PubMed: 15592819]
5. Zhang WD, Evans DH. Detection and identification of human influenza viruses by the polymerase chain reaction. *J Virol Methods*. 1991; 33:165–89. [PubMed: 1939505]
6. Killian ML. Hemagglutination assay for the avian influenza virus. *Methods Mol Biol*. 2008; 436:47–52. [PubMed: 18370040]
7. Gamblin SJ, Haire LF, Russell RJ, Stevens DJ, Xiao B, Ha Y, Vasisht N, Steinhauer DA, Daniels RS, Elliot A, Wiley DC, Skehel JJ. The structure and receptor binding properties of the 1918 influenza hemagglutinin. *Science*. 2004; 303:1838–42. [PubMed: 14764886]
8. Lu B, Zhou H, Ye D, Kembler G, Jin H. Improvement of influenza A/Fujian/411/02 (H3N2) virus growth in embryonated chicken eggs by balancing the hemagglutinin and neuraminidase activities, using reverse genetics. *J Virol*. 2005; 79:6763–71. [PubMed: 15890915]

9. Medeiros R, Escriou N, Naffakh N, Manuguerra JC, van der Werf S. Hemagglutinin residues of recent human A(H3N2) influenza viruses that contribute to the inability to agglutinate chicken erythrocytes. *Virology*. 2001; 289:74–85. [PubMed: 11601919]
10. Nobusawa E, Ishihara H, Morishita T, Sato K, Nakajima K. Change in receptor-binding specificity of recent human influenza A viruses (H3N2): a single amino acid change in hemagglutinin altered its recognition of sialyloligosaccharides. *Virology*. 2000; 278:587–96. [PubMed: 11118381]
11. Chandrasekaran A, Srinivasan A, Raman R, Viswanathan K, Raguram S, Tumpey TM, Sasisekharan V, Sasisekharan R. Glycan topology determines human adaptation of avian H5N1 virus hemagglutinin. *Nat Biotechnol*. 2008; 26:107–13. [PubMed: 18176555]
12. Srinivasan A, Viswanathan K, Raman R, Chandrasekaran A, Raguram S, Tumpey TM, Sasisekharan V, Sasisekharan R. Quantitative biochemical rationale for differences in transmissibility of 1918 pandemic influenza A viruses. *Proc Natl Acad Sci U S A*. 2008; 105:2800–5. [PubMed: 18287068]
13. Shriver Z, Raman R, Viswanathan K, Sasisekharan R. Context-specific target definition in influenza A virus hemagglutinin-glycan receptor interactions. *Chem Biol*. 2009; 16:803–14. [PubMed: 19716471]
14. Tretter V, Altmann F, Marz L. Peptide-N4-(N-acetyl-beta-glucosaminyl)asparagine amidase F cannot release glycans with fucose attached alpha 1----3 to the asparagine-linked N-acetylglucosamine residue. *Eur J Biochem*. 1991; 199:647–52. [PubMed: 1868849]
15. Zaia J. Mass spectrometry and the emerging field of glycomics. *Chem Biol*. 2008; 15:881–92. [PubMed: 18804025]
16. Zaikin VG, Halket JM. Derivatization in mass spectrometry--8. Soft ionization mass spectrometry of small molecules. *Eur J Mass Spectrom (Chichester, Eng)*. 2006; 12:79–115.
17. Mechref Y, Novotny MV. Matrix-assisted laser desorption/ionization mass spectrometry of acidic glycoconjugates facilitated by the use of spermine as a co-matrix. *J Am Soc Mass Spectrom*. 1998; 9:1293–302. [PubMed: 9835074]
18. Ito T, Suzuki Y, Mitnaul L, Vines A, Kida H, Kawaoka Y. Receptor specificity of influenza A viruses correlates with the agglutination of erythrocytes from different animal species. *Virology*. 1997; 227:493–9. [PubMed: 9018149]
19. Stevens J, Blixt O, Paulson JC, Wilson IA. Glycan microarray technologies: tools to survey host specificity of influenza viruses. *Nat Rev Microbiol*. 2006; 4:857–64. [PubMed: 17013397]
20. Rogers GN, D'Souza BL. Receptor binding properties of human and animal H1 influenza virus isolates. *Virology*. 1989; 173:317–22. [PubMed: 2815586]
21. Connor RJ, Kawaoka Y, Webster RG, Paulson JC. Receptor specificity in human, avian, and equine H2 and H3 influenza virus isolates. *Virology*. 1994; 205:17–23. [PubMed: 7975212]
22. Uchida Y, Tsukada Y, Sugimori T. Enzymatic properties of neuraminidases from *Arthrobacter ureafaciens*. *J Biochem*. 1979; 86:1573–85. [PubMed: 42648]
23. Fournet B, Montreuil J, Strecker G, Dorland L, Haverkamp J, Vliegenthart FG, Binette JP, Schmid K. Determination of the primary structures of 16 asialo-carbohydrate units derived from human plasma alpha 1-acid glycoprotein by 360-MHZ 1H NMR spectroscopy and permethylation analysis. *Biochemistry*. 1978; 17:5206–14. [PubMed: 728395]
24. Dorland L, Haverkamp J, Vliegenthart JF. Determination by 360 MHz 1H NMR spectroscopy of the type of branching in complex asparagine-linked glycan chains of glycoproteins. *FEBS Lett*. 1978; 89:149–52. [PubMed: 658393]
25. Dorland L, Haverkamp J, Vliegenthart JF, Strecker G, Michalski JC, Fournet B, Spik G, Montreuil J. 360-MHZ 1H nuclear-magnetic-resonance spectroscopy of sialyl-oligosaccharides from patients with sialidosis (mucopolipidosis I and II). *Eur J Biochem*. 1978; 87:323–9. [PubMed: 668697]
26. Strecker G, Fournet B, Montreuil J. Structure of the three major fucosyl glycoasparagines accumulating in the urine of a patient with fucosidosis. *Biochimie*. 1978; 60:725–34. [PubMed: 728478]
27. (a) Halbeek HV. *Methods Mol Biol*. 1993; 17:115–148. [PubMed: 21400136] (b) Di Patrizi L, Rosati F, Guerranti R, Pagani R, Gerwig GJ, Kamerling JP. Structural characterization of the N-glycans of gpMuc from *Mucuna pruriens* seeds. *Glycoconj. J*. 2006; 23:599–609. [PubMed:

- 17006651] (c) Koles K, van Berkel PH, Pieper FR, Nuijens JH, Mannesse ML, Vliegthart JF, Kamerling JP. N- and O-glycans of recombinant human C1 inhibitor expressed in the milk of transgenic rabbits. *Glycobiology*. 2004; 14:51–64. [PubMed: 14514717] (d) Di Patrizi L, Capone A, Focarelli R, Rosati F, Gallego RG, Gerwig GJ, Vliegthart JF. Structural characterization of the N-glycans of gp273, the ligand for sperm-egg interaction in the mollusc bivalve *Unio elongatulus*. *Glycoconj. J.* 2001; 18:511–518. [PubMed: 12151712] (e) Leeflang BR, Faber EJ, Erbel P, Vliegthart JF. Structure elucidation of glycoprotein glycans and of polysaccharides by NMR spectroscopy. *J. Biotechnol.* 2000; 77:115–122. [PubMed: 10674218]
28. Guile GR, Rudd PM, Wing DR, Prime SB, Dwek RA. A rapid high-resolution high-performance liquid chromatographic method for separating glycan mixtures and analyzing oligosaccharide profiles. *Anal Biochem.* 1996; 240:210–26. [PubMed: 8811911]
29. Green ED, Baenziger JU. Asparagine-linked oligosaccharides on lutropin, follitropin, and thyrotropin. I. Structural elucidation of the sulfated and sialylated oligosaccharides on bovine, ovine, and human pituitary glycoprotein hormones. *J Biol Chem.* 1988; 263:25–35. [PubMed: 3121609]
30. Duk M, Krotkiewski H, Stasyk TV, Lutsik-Kordovsky M, Syper D, Lisowska E. Isolation and characterization of glycophorin from nucleated (chicken) erythrocytes. *Arch Biochem Biophys.* 2000; 375:111–8. [PubMed: 10683255]
31. Song X, Lasanajak Y, Xia B, Smith DF, Cummings RD. Fluorescent glycosylamides produced by microscale derivatization of free glycans for natural glycan microarrays. *ACS Chem Biol.* 2009; 4:741–50. [PubMed: 19618966]



**Fig. 1. MALDI-TOF mass spectra of free, non-reduced N-glycans isolated from cRBCs**  
 Peaks appeared in the mass range of 2000 to 3600 with the most prominent peaks at  $m/z$  2589.1 and 2880.5. Each peak was calibrated as a non-sodiated species using external N-glycan standards as mass calibrants. Proposed glycan structures for each peak using MS annotation software are shown along with their observed  $m/z$  value. The number in the bracket for each glycan indicates the percentage of each corresponding glycan within the total glycan pool as estimated by semi-quantitative MALDI MS.



**H3-eq, C3H  
of  $\alpha(2 \rightarrow 3)$   
NeuAc  
(54 %)**

**H3-eq, C3H  
of  $\alpha(2 \rightarrow 6)$   
NeuAc  
(46 %)**

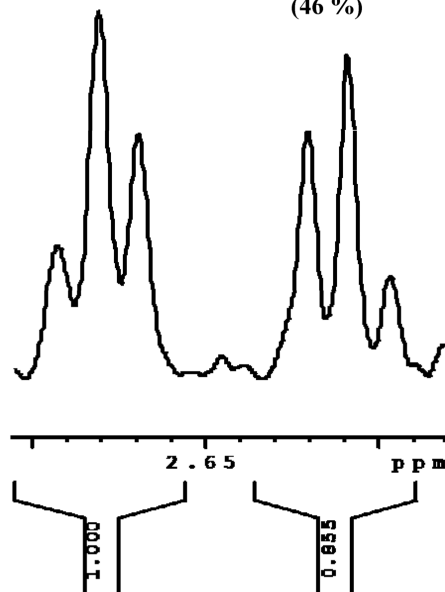
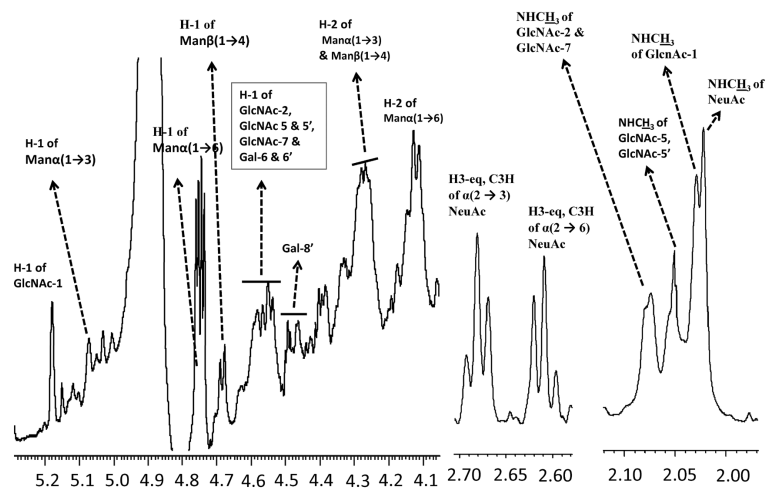


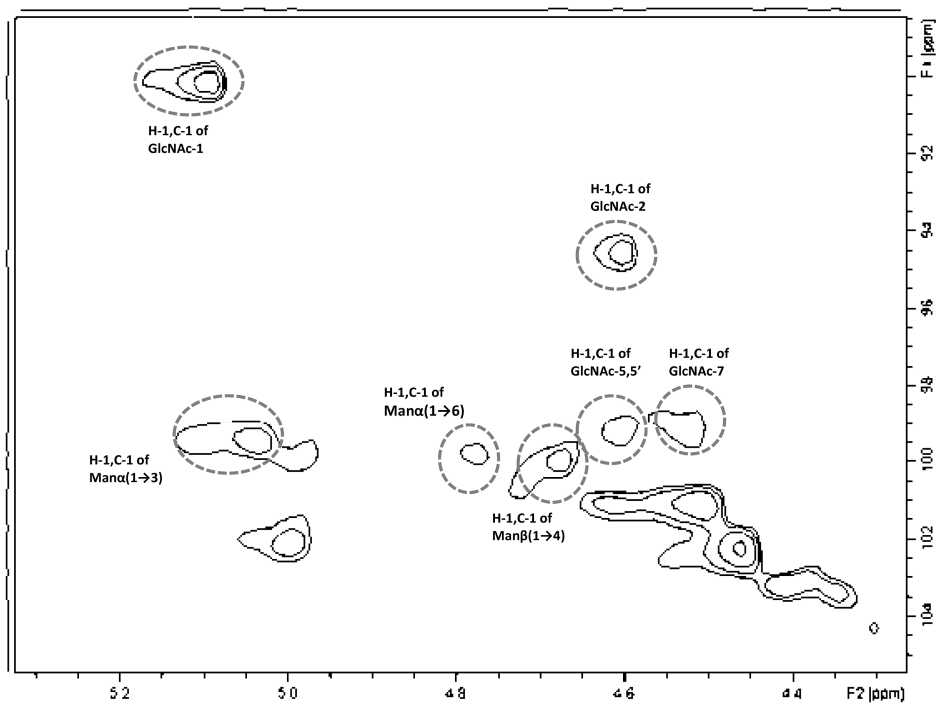
Fig. 2. Qualitative and quantitative linkage analysis of N-glycans from cRBCs



(A) MALDI-MS spectra of sialidase S-treated, unlabeled, N-glycans that were released from cRBCs by PNGase F. (B)  $^1\text{H-NMR}$  spectra of sialic acid linkage in the free non reduced N-glycans isolated from cRBCs.

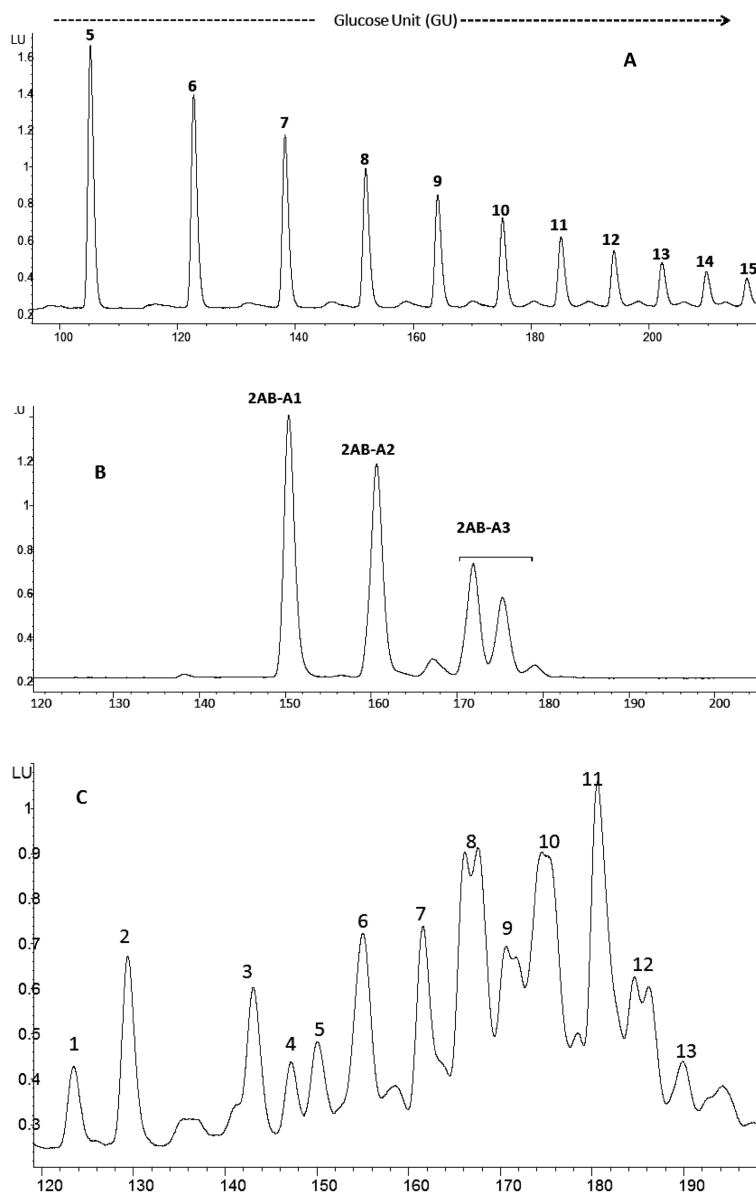


**Fig. 3.**  $^1\text{H-NMR}$  (600 MHz,  $\text{D}_2\text{O}$ ) spectra of N-glycans from cRBCs  
 Landmark chemical shifts are identified for each region of interest. The possible structural annotations of each monosaccharide fingerprint proton are labeled in the spectrum.



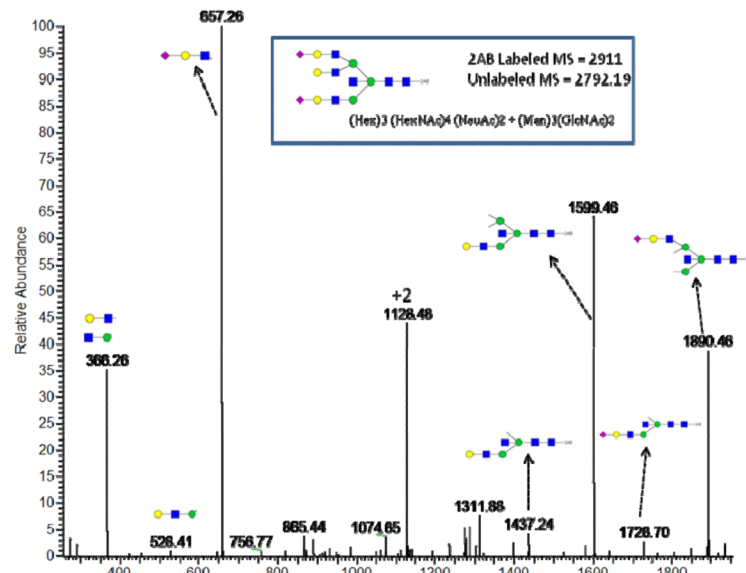
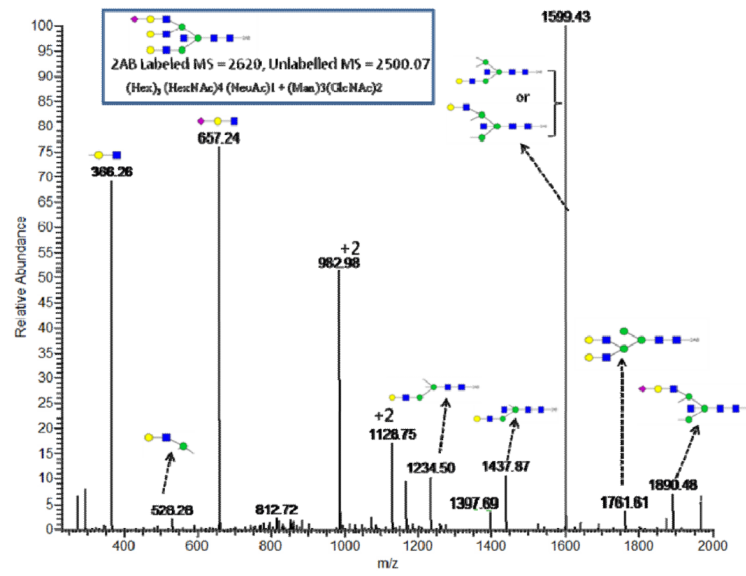
**Fig. 4. HSQC-spectra of N-glycans from cRBCs**

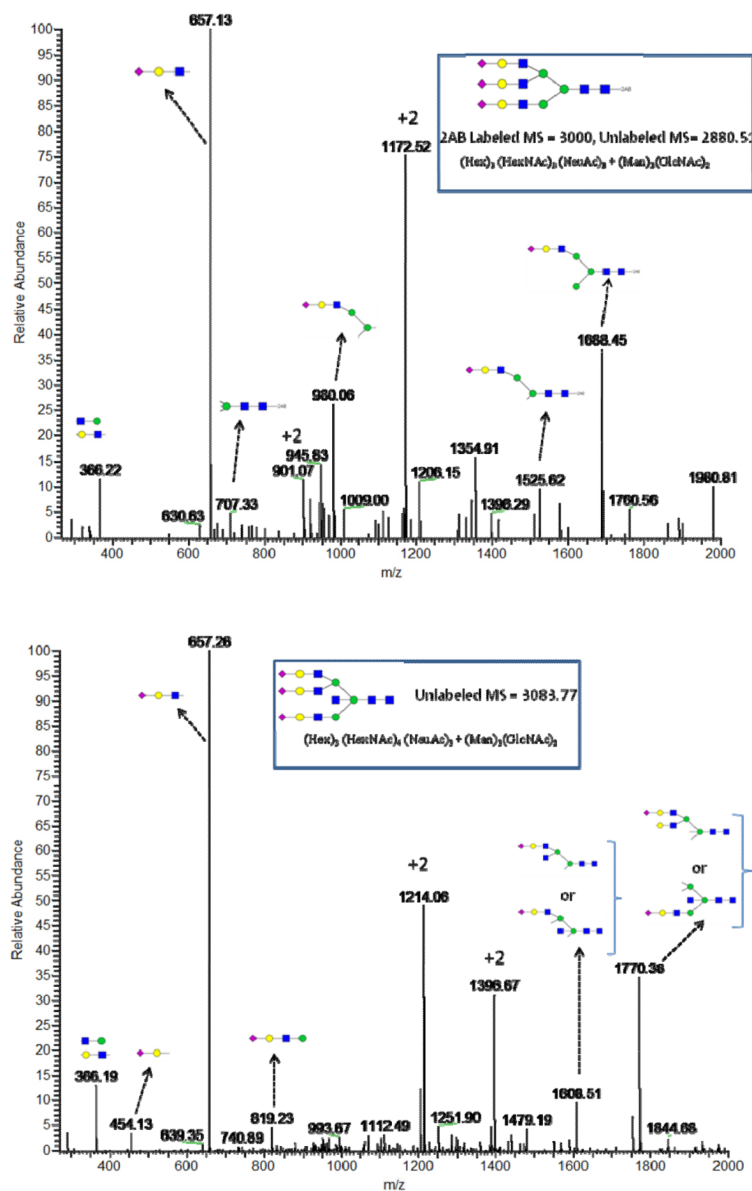
The spectrum shows the cross peaks between the anomeric protons (5.25–4.30 ppm) and carbon (89–105 ppm) signals. The cross peaks confirm the presence of primarily bi- and triantennary structures. Notably, there is no cross peak detected at around 4.68–4.71 ppm, indicating the absence of lactosamine repeat units in the cRBC N-glycan pool.



**Fig. 5. HPLC profiling of 2AB-linked N-glycan isolated from cRBCs**

Glycans are eluted using a normal phase column with a 50 mM ammonium formate/ acetonitrile gradient as eluant. Total run time is 290 minutes. (A) HPLC profiling of glucose homo-polymer for calibration of the column. (B) A mixture of three sialic acid containing N-glycans standards, chosen based on their polarity and molecular weight, are used as benchmarks. Three different species appeared in the retention time between 120–200 min. (C) 2-AB labeled N-glycan pool from cRBCs were analyzed within the calibrated and standardized column system. The acidic N-glycans from cRBCs eluted within the retention time window of 120–200 minutes. Glycan under each peak was determined from the MALDI-MS data of the isolated fraction of their corresponding peaks (Table S3).

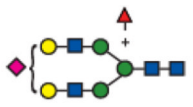
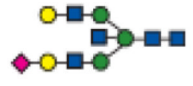
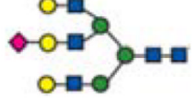

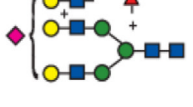

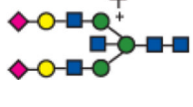
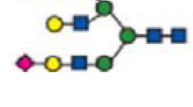
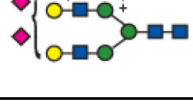
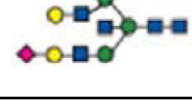


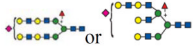
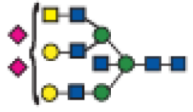
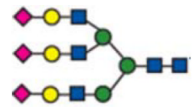
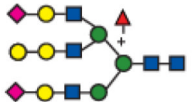
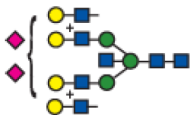
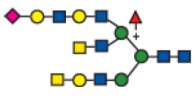
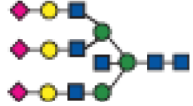


**Fig. 6. LC-MS/MS data of selected MS peaks of N-glycans from cRBC**  
 Shown are the MS/MS signals of 2-AB labeled structures: (A) 2620; (B) 2911; (C) 3000; and unlabeled structure: (D) 3083.8. Fragment assignments are shown for each structure.

**Table 1**

Structural assignment of the major N-glycans from cRBCs and comparison to those observed in human bronchial epithelial cells (HBE's).

Theoretical Molecular Mass	Molecular Structure	N-Glycan Source	
		HBEs	cRBCs
2077.7		Present	Absent
2134.8		Absent	Present
2296.8		Present	Present
2422.8		Absent	Present
2442.9		Present	Absent
2499.9		Absent	Present
2571.9		Present	Minor
2587.9		Present	Present
2734.0		Present	Absent
2791.0		Absent	Present

Theoretical Molecular Mass	Molecular Structure	N-Glycan Source	
		HBEs	cRBCs
2808.0		Present	Absent
2832.0		Absent	Present
2879.0		Minor	Present <sup>§</sup>
2896.0		Present	Absent
2953.0		Present	Minor
3052.1		Present	Absent
3082.1		Absent	Present